N-Hydroxypyrazolyl Glycine Derivatives as Selective *N*-Methyl-D-aspartic Acid Receptor Ligands

Rasmus P. Clausen,*[,†] Caspar Christensen,[†] Kasper B. Hansen,[†,‡,||] Jeremy R. Greenwood,[†] Lars Jørgensen,[†] Nicola Micale,[†] Jens Christian Madsen,[§] Birgitte Nielsen,[†] Jan Egebjerg,[||] Hans Bräuner-Osborne,[†] Stephen F. Traynelis,[‡] and Jesper L. Kristensen[†]

Department of Medicinal Chemistry, Faculty of Pharmaceutical Sciences, University of Copenhagen, 2 Universitetsparken, DK-2100 Copenhagen, Denmark, Department of Pharmacology, Emory University School of Medicine, Rollins Research Center, Atlanta, Georgia, Department of Medicinal Chemistry and Department of Molecular Neurobiology, H. Lundbeck A/S, 9 Ottiliavej, DK-2500 Valby, Denmark

Received January 15, 2008

A series of analogues based on *N*-hydroxypyrazole as a bioisostere for the distal carboxylate group of aspartate have been designed, synthesized, and pharmacologically characterized. Affinity studies on the major glutamate receptor subgroups show that these 4-substituted *N*-hydroxypyrazol-5-yl glycine (NHP5G) derivatives are selectively recognized by *N*-methyl-D-aspartic acid (NMDA) receptors and that the (*R*)-enantiomers are preferred. Moreover, several of the compounds are able to discriminate between individual subtypes among the NMDA receptors, providing new pharmacological tools. For example, 4-propyl NHP5G is an antagonist at the NR1/NR2A subtype but an agonist at the NR1/NR2D subtype. Molecular docking studies indicate that the substituent protrudes into a region that may be further exploited to improve subtype selectivity, thereby opening up a design strategy for ligands which can differentiate individual NMDA receptor subtypes.

Introduction

The glutamate receptors (GluRs) are a group of receptors with a prominent role in neurotransmission because most of the excitatory signals in the brain are mediated by glutamic acid (Glu, Figure 1).[1–3] These receptors are involved in key processes of the central nervous system (CNS) such as learning and memory[4] but are also implicated in several neuropathological conditions such as ischemia, epilepsy, schizophrenia, chronic pain, and Alzheimer's disease.[5] Therefore, the GluRs have been the target of extensive research for more than three decades, and one of the goals has been to develop compounds that can alter glutamatergic neurotransmission in a selective manner. Such compounds have been and continue to be important tools in discovering new therapeutic possibilities and to gain a functional understanding of this group of receptors.[6,a]

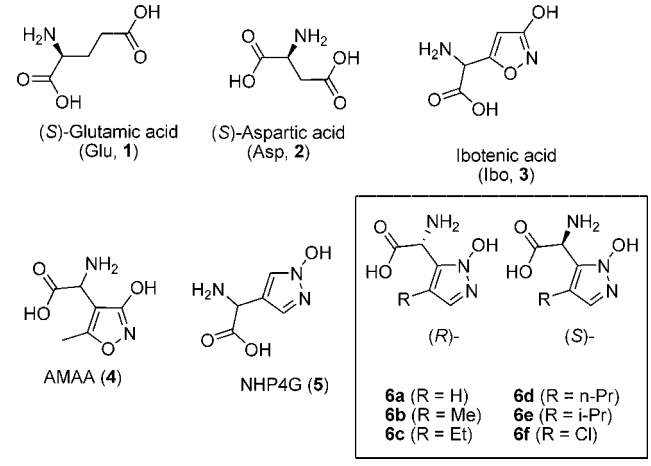

Figure 1. Structures of the excitatory amino acids glutamic acid and aspartic acid and bioisosteric analogues of these compounds with activity at the glutamate receptors.

Two different signaling pathways divide the GluRs: metabotropic glutamate receptors (mGluRs) are G-protein-coupled receptors that mediate slow modulatory responses, and ionotropic glutamate receptors (iGluRs) are cation-conducting ion channels that mediate fast neurotransmission via depolarization of the membrane potential. Based on activation by selective ligands and cDNA homology, the iGluRs are divided into *N*-methyl-D-aspartic acid (NMDA), (*S*)-2-amino-3-(3-hydroxy-5-methyl-4-isoxazolyl)propionic acid (AMPA), and kainic acid (KA) receptors. The iGluRs are homo- or heteromeric assemblies of four subunits. Seven NMDA subunits (NR1, NR2A-D, NR3A, NR3B), four AMPA (GluR1−4), and five KA (GluR5−7 and KA1−2) preferring subunits have been identified.[1] NMDA glutamate receptors are assembled from two NR1 subunits and two NR2 subunits and are activated by the simultaneous binding of glycine and glutamate to the NR1 and NR2 subunits, respectively. NR3 subunits also can coassemble with NMDA receptors, although the stoichiometry is unclear.

The iGluR subunit consists of an intracellular C-terminal domain, a transmembrane domain that forms the ion channel pore, and a pair of extracellular domains: the agonist binding domain (ABD) and the N-terminal domain. Over the past decade, an increasing number of X-ray crystal structures of the ABDs of the GluRs have appeared (86 available structures to

* To whom correspondence should be addressed. Phone: +45 35 33 65 66. Fax: +45 35 33 60 40. E-mail: rac@farma.ku.dk.
† Department of Medicinal Chemistry, Faculty of Pharmaceutical Sciences, University of Copenhagen.
‡ Department of Pharmacology, Emory University School of Medicine, Rollins Research Center.
§ Department of Medicinal Chemistry, H. Lundbeck A/S.
|| Department of Molecular Neurobiology, H. Lundbeck A/S.

[a] Abbreviations: NHP5G, 2-(*N*-hydroxypyrazol-5-yl)glycine, 2-(*N*-hydroxypyrazol-4-yl)glycine; NMDA, *N*-methyl-D-aspartic acid; GluRs, glutamate receptors; Glu, glutamate; CNS, central nervous system; mGluRs, metabotropic glutamate receptors; iGluRs, ionotropic glutamate receptors; AMPA, (*S*)-2-amino-3-(3-hydroxy-5-methyl-4-isoxazolyl)propionic acid; KA, kainic acid; ABD, agonist binding domain; AMAA, (*R*,*S*)-2-amino-2-(3-hydroxy-5-methyl-4-isoxazolyl)acetic acid.

10.1021/jm800025e CCC: $40.75
Published on Web 06/25/2008

date, covering all the major mammalian subtypes as well as bacterial homologues), providing detailed structural knowledge of agonist binding and the molecular pharmacology of this group of receptors.[3,7–11] These crystallographic structures have shown that iGluR ABDs are clamshell-like structures, where the agonist binds in the cleft formed by two lobes. Upon agonist binding, the two lobes close around the agonist, whereas binding of antagonists stabilizes an open domain structure. Furthermore, the extent to which substituents on AMPA receptor ligands promote domain closure at the GluR2 ABD correlates with the degree of receptor activation.[12,13] By contrast, crystallographic structures of the NR1 ABD, which hosts the binding site of the NMDA receptor coagonist glycine, have revealed that the degree of ABD closure is the same for partial and full agonists at the glycine site.[14] Nevertheless, a correlation between the steric requirements of the ligand and the extent of receptor activation still seems to exist because series of carbocyclic agonists show decreasing efficacy with the size of the ring (cyclopropylglycine > cyclobutylglycine > cyclopentylglycine).

We and co-workers have previously reported the synthesis and pharmacological characterization of a series of 5-substituted (*R*,*S*)-2-(*N*-hydroxypyrazol-4-yl)glycine ((*R*,*S*)-NHP4G, (**5**) analogues as GluR ligands.[15,16] These glutamic acid analogues are structurally related to the naturally occurring excitotoxin ibotenic acid (Ibo, **3**), but with an *N*-hydroxypyrazole instead of a 3-hydroxyisoxazole moiety as the bioisosteric substitute for the distal carboxylic acid of Glu. The unsubstituted analogue (*R*,*S*)-NHP4G displayed activity at several GluRs, but the pharmacological profile narrowed upon substitution, limiting the activity to group II mGluRs and NMDA receptors. Even small substituents at the 5-position of the partial NMDA agonist (*R*,*S*)-NHP4G turned these compounds into antagonists at NMDA receptors. Recently, we expanded this series[17] to include aspartic acid analogues such as the unsubstituted (*R*,*S*)-2-(*N*-hydroxypyrazol-5-yl)glycine analogue ((*R*,*S*)-NHP5G, **6a**). This compound (**6a**) is a selective NMDA receptor partial agonist, like the structurally related NMDA receptor agonist (*R*,*S*)-2-amino-2-(3-hydroxy-5-methyl-4-isoxazolyl)acetic acid AMAA (**4**), whereas 4-aryl NHP5G analogues are antagonists.

We have extended the NHP5G series and separated enantiomers in order to establish the steric requirements for the pharmacological behavior of these derivatives. Compounds **6a** and **6f** from this series have already been applied in an extensive mutation study[18] in order to establish the structural determinants that could account for the partial agonism at the NR1/NR2B receptor subtype. The synthesis and pharmacological characterization of a larger 4-substituted NHP5G series will be presented here.

Results

Chemistry. The synthesis of the compounds (Scheme 1) started from *O*-benzyl protected *N*-hydroxypyrazole **7**, which is iodinated, yielding **8** as previously described.[19] Metal−halogen exchange converts **8** into a Grignard reagent with isopropyl magnesium chloride, which then reacts with various aldehydes and ketones, yielding alcohols **9a**−**9d**. These alcohols are deoxygenated by treatment with TFA and triethylsilane, giving 4-substituted hydroxypyrazoles **10a**−**10d**. The chloro substituted compound **10e** is obtained directly from **7** by treatment with sulfuryl chloride. Selective lithiation followed by treatment with the amino acid synthon diethyl *N*-Boc iminomalonate yields protected amino diesters **11a**−**e**, which are debenzylated by hydrogenation, yielding **12a**−**e**. Ester hydrolysis followed by acidic removal of the Boc group and concomitant spontaneous decarboxylation yields racemic amino acids **6b**−**f**. The enantiomers could be separated by chiral HPLC, thus enabling a preparative resolvation of the compounds including NHP5G. Because the mobile phase was diluted aqueous TFA, the enantiomers were isolated as TFA salts, containing varying amounts of TFA. The amount of TFA was determined by NMR spectroscopy using the ERETIC technique,[20] where an electronically generated signal serves as a quantification reference. For TFA, the ERETIC technique must be applied to ^{19}F NMR spectroscopy because the absence of nonlabile protons makes ^{1}H NMR unsuitable in this case. However, the compounds studied here are void of fluorine nuclei, so quantification relative to TFA necessitates the use of an ERETIC signal in both the ^{1}H and the ^{19}F NMR spectra. The relative strength of the ^{1}H and ^{19}F ERETIC signals must then be calibrated using a compound containing both protons and fluorine. For this purpose, we used a sample of citalopram oxalate. In general, the content of TFA was less than 1 equivalent.

Scheme 1[a]

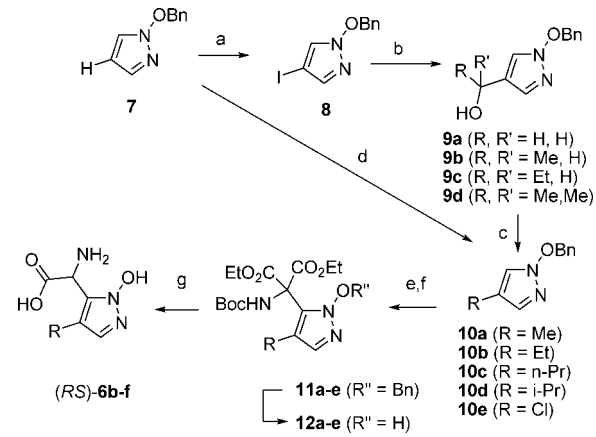

[a] Reagents and conditions: (a) I−Cl; (b) (1) *i*-PrMgCl, −78°C, THF; (2) RC═OR′; (c) TFA, Et_3SiH; (d) SO_2Cl_2 (for **10e**); (e) (1) n-BuLi, −78°C; (2) diethyl *N*-Boc iminomalonate; (f) H_2, Pd/C, MeOH; (g) (1) LiOH; (2) HCl.

Determination of Absolute Configuration. We were unable to obtain crystals suitable for X-ray structure determination of any of the compounds and therefore we turned to a number of other methods in order to determine the absolute configuration. First, the elution order on the chiral HPLC column clearly indicated the absolute stereochemistry for all the compounds (Figure 2). Thus, the L-form of α-amino acids generally elutes before the D-form on a CR(−) Crownpak chiral column, corresponding to the (*S*)- and (*R*)-enantiomer, respectively.[21,22]

Second, we turned to the electronic circular dichroism (ECD) spectra. Traditionally, an empirical correlation has been noted between the *S*-isomer of aryl amino acids and observation of a positive Cotton effect in the ECD.[23] However, in recent years, prediction of the ECD spectrum has become tractable from first principles using methods such as time-dependent density functional theory (TD-DFT), reducing the reliance on empiricism for interpretation. Thus, to obtain further evidence for the absolute configuration, CD spectra (Figure 3) of at least one enantiomer of **6b**−**6f** were therefore recorded and in the case of (*S*)-Cl-NHP5G (**6f**) compared with that calculated using TD-DFT for eight low energy conformers in dilute acidic aqueous solution (Figure 3). Although the first major peak according to the Boltzmann average lies approximately 20 nm lower in energy than observed, the magnitude was in good agreement with experiment and indicative of the same correlation as usually seen. Although the exact shape of the predicted peak depends

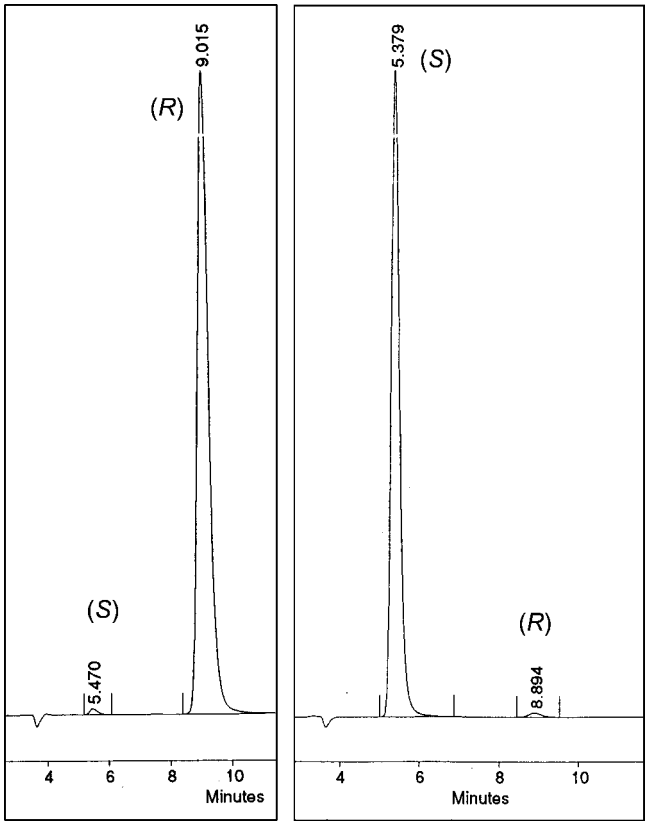

Figure 2. Two chiral HPLC chromatograms of (*S*)- and (*R*)-**6d**, respectively, showing the elution order on an analytical Crownpak CR(−) column. The order is reversed on a preparative Crownpak CR(+) column.

on the weighting of the conformers, and is thus highly sensitive to the accuracy of conformational energies, the small experimental negative peak at around 230 nm for (*S*)-**6f** was also visible in two of the four lowest energy conformers and in agreement with that previously observed for phenylglycine.[23] Comparing (*S*)-**6b** with (*S*)-**6f** showed that there was no significant qualitative difference between the calculated spectra or between any of the experimental spectra, and thus it is reasonable to expect the correlation to hold throughout this series.

Finally, we prepared the Mosher amide of (*S*)-**6c** and compared the NMR spectra of the two diastereomers with the isotropic magnetic shielding values calculated for the hydrogen nuclei using DFT. Because these amide derivatives have several rotatable bonds, spectra were calculated for the hundred lowest energy conformers of both (*S*,*S*) and (*R*,*S*), according to a conformational search with OPLS2005. Although qualitative agreement was noted, the precise differences in the calculated shifts between the diastereomers again proved highly sensitive to conformational energies when using a Boltzmann weighted average. We therefore calculated regression coefficients between the shifts in the two experimental proton spectra and the 200 calculated spectra. For a majority of the calculated (*R*,*S*) conformers, the calculated spectrum was a better match for (*R*,*S*) than (*S*,*S*), and for a majority of the calculated (*S*,*S*) conformers, the calculated spectrum was a better match for experimental (S,S). Moreover, for the single conformers of (*R*,*S*) and (*S*,*S*) with the highest regression coefficients, the calculated (*R*,*S*) spectrum was a better match for experimental (*R*,*S*) spectrum (R^2 = 0.9993) and vice versa for (*S*,*S*) (R^2 = 0.9985). The absolute configurations are therefore assigned on the basis of

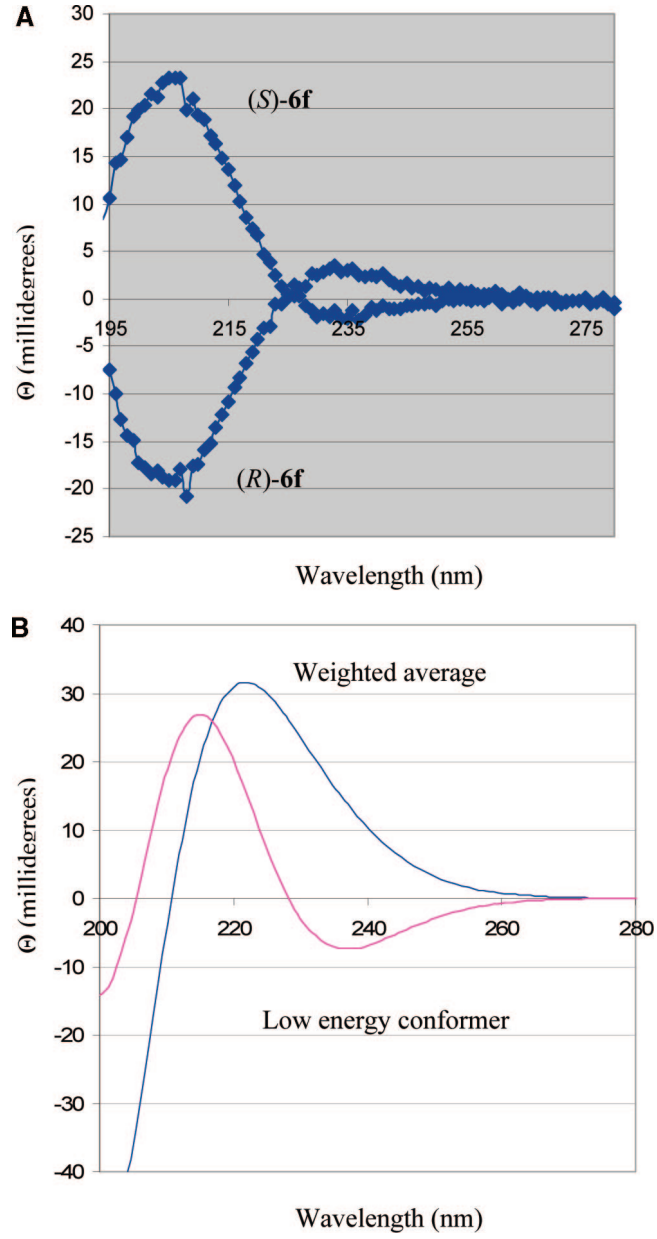

Figure 3. Electronic circular dichroism spectra (A) of compounds (*R*)- and (*S*)-**6f** at a concentration of 0.325 mg/mL in H_2O compared with a TD-DFT simulated spectra (B) of a weighted average of eight low energy conformers as well as a single low energy conformer of (*S*)-**6f** in dilute acid.

three independent types of experiment, interpreted by a combination of empirical and first-principles correlations.

Pharmacology. First we investigated the affinity of the compounds for the major iGluR subgroups. As shown in Table 1, all the analogues are selective NMDA receptor ligands with affinity in the low micromolar range. Furthermore, the affinity was found to reside with the (*R*)-enantiomer of the compounds, the most potent being (*R*)-**6a**, (*R*)-**6b**, and (*R*)-**6f**.

The affinity at NMDA receptors prompted functional characterization at recombinant NMDA receptors expressed in *Xenopus laevis* oocytes to determine whether the compounds could discriminate between individual subtypes (Table 2, Figures 4 and 5).

Compounds (*R*,*S*)-**6c**, (*R*,*S*)-**6d**, and (*R*,*S*)-**6f** acted as partial agonists on four NMDA receptor subunit combinations (NR1/NR2A, NR1/NR2B, NR1/NR2C, and NR1/NR2D) but with

Table 1. Receptor Binding Affinities of Compounds **6a**−**6f** at Three Major Groups of iGluRs in Rat Cortical Synaptosome Assay[a,24]

		IC_{50} (μM)		K_i (μM)
compd	R	[^{3}H]AMPA	[^{3}H]KAIN	[^{3}H]CGP39653
Glu		0.34[b]	0.38[b]	0.20[b]
(*R*,*S*)-**6a**	H	>100	>100	10 [9, 11][b]
(*R*)-**6a**		>100	>100	2.2 [2.0, 2.4]
(*S*)-**6a**		>100	>100	>100
(*R*,*S*)-**6b**	Me	>100	>100	22 [20, 24]
(*R*)-**6b**		>100	>100	2.2 [2.1, 2.4]
(*S*)-**6b**		>100	>100	>100
(*R*,*S*)-**6c**	Et	>100	>100	13 [11, 15]
(*R*)-**6c**		>100	>100	4.4 [3.3, 5.7]
(*S*)-**6c**		>100	>100	>100
(*R*,*S*)-**6d**	n-Pr	>100	>100	14 [14, 15]
(*R*)-**6d**		>100	>100	6.9 [5.9, 8.2]
(*S*)-**6d**		>100	>100	>100
(*R*,*S*)-**6e**	i-Pr	>100	>100	20 [19, 21]
(*R*)-**6e**		>100	>100	13 [11, 16]
(*S*)-**6e**		>100	>100	>100
(*R*,*S*)-**6f**	Cl	>100	>100	2.9 [2.7, 3.2]
(*R*)-**6f**		ND[c]	ND	2.9 [2.6, 3.2]
(*S*)-**6f**		>100	>100	25 [24, 26]

[a] The numbers in brackets [min, max] indicate mean ± SEM according to a logarithmic distribution. [b] Ref 16. [c] ND: not determined.

Table 2. Potency and Efficacy Relative to Glu of Compounds **6a**, **6c**, **6d**, and **6f** at Recombinant NR1/NR2A-D Receptors Expressed in *Xenopus* Oocytes[a,24]

compound	R	subtype	EC_{50} (μM)	rel I_{max}	n_{Hill}
Glu[b]		NR1/NR2A	2.9	1	1.5
		NR1/NR2B	1.8	1	1.7
		NR1/NR2C	1.0	1	1.3
		NR1/NR2D	0.45	1	1.6
NMDA[b]		NR1/NR2A	75	0.90 ± 0.04	1.5
		NR1/NR2B	22	0.77 ± 0.01	1.4
		NR1/NR2C	23	0.73 ± 0.02	1.4
		NR1/NR2D	8.3	0.80 ± 0.02	1.6
(*R*,*S*)-**6a**[c]	H	NR1/NR2A	82 [75, 90]	0.45 ± 0.03	1.3
		NR1/NR2B	48 [47, 49]	0.58 ± 0.02	1.6
		NR1/NR2C	54 [50, 57]	0.52 ± 0.01	1.4
		NR1/NR2D	ND[d]	ND	ND
(*R*,*S*)-**6c**	Et	NR1/NR2A	47 [39, 57]	0.05 ± 0.01	2.4
		NR1/NR2B	68 [64, 72]	0.45 ± 0.06	1.2
		NR1/NR2C	91 [82, 101]	0.52 ± 0.03	1.3
		NR1/NR2D	43 [42, 44]	0.70 ± 0.03	1.5
(*R*,*S*)-**6d**	*n*-Pr	NR1/NR2A	NA[d]	NA	NA
		NR1/NR2B	105 [95, 116]	0.06 ± 0.01	1.9
		NR1/NR2C	429 [367, 500]	0.22 ± 0.02	1.1
		NR1/NR2D	153 [142, 165]	0.37 ± 0.02	1.6
(*R*,*S*)-**6f**	Cl	NR1/NR2A	565 [464, 687]	0.07 ± 0.03	3.2
		NR1/NR2B	149 [139, 160]	0.29 ± 0.01	1.2
		NR1/NR2C	255 [250, 260]	0.55 ± 0.01	1.4
		NR1/NR2D	152 [149, 155]	0.73 ± 0.02	1.4

[a] Data are from 3−5 oocytes and the numbers in brackets [min, max] indicate mean ± SEM according to a logarithmic distribution. [b] Ref 38. [c] Ref 16. [d] NA: no activity; ND: not determined.

highly varying potency and agonist efficacy at the different subtypes. At NR2A-containing receptors, the ethyl substituted (*R*,*S*)-**6c** and chloro substituted (*R*,*S*)-**6f** are low-efficacy partial agonists, but (*R*,*S*)-**6c** is an order of magnitude more potent than (*R*,*S*)-**6f**. (*R*,*S*)-**6d** displayed antagonist activity at NR1/NR2A ($n = 5$) but was an agonist on all other subtypes (Figure 5) and is thus the compound showing the largest difference among subtypes in this series. At NR1/NR2B (*R*,*S*)-**6c** and (*R*,*S*)-**6f** were approximately equipotent and had higher agonist efficacies than at NR1/NR2A, but the efficacies varied more. By contrast, compounds (*R*,*S*)-**6c** and (*R*,*S*)-**6f** showed similar agonist efficacy relative to Glu around 0.5 at NR2C and 0.7 at NR2D, and again compound (*R*,*S*)-**6c** was more potent than (*R*,*S*)-**6f**.

In our previous study including compounds (*R*)-**6a** and (*R*)-**6f**, ligand variation was matched against corresponding mutations in the receptor, leading to the conclusion that the degree of agonist efficacy relative to Glu correlates inversely with the steric bulk introduced into the agonist binding pocket, either by the ligand or in the receptor by mutation. It was therefore interesting to see whether this dependence would manifest in the present series too. The *R*-enantiomer of compounds **6a**−**d** and **6f** was therefore characterized at NR1/NR2B (Table 3 and Figure 6; see also Supporting Information). However, the relative agonist efficacy of the compounds did not show a simple correlation with the nature of the substituents. Thus, the unsubstituted NHP5G (**6a**) induced a fraction of 0.61 of the Glu-induced current and compounds with methyl-(**6b**) and *n*-propyl-substituents (**6d**) displayed markedly lower relative efficacies of 0.23 and 0.09, respectively. The chloro substituted compound (**6f**) was slightly more efficacious (0.33) than the methyl substituted compounds, but the ethyl substituted compound (**6c**) induced a 0.46 current relative to the Glu current, which is twice that of the methyl substituted compound and which is notable because an ethyl substituent is more bulky than a methyl substituent. The isopropyl substituted compound (**6e**) was an antagonist at NR1/NR2B (see Supporting Information).

Molecular Modeling. To understand the unexpected trend in the agonist efficacies of this series of 4-substituted NHP5G, we docked the compounds in a homology model of the ABD of NR2B using the recently published X-ray structure of the ABD of NR2A (PDB code 2A5S) as a template.[25] In our recent mutation study, the homology model was based on a NR1 crystallographic structure (PDB code 1PB7), but the new X-ray structure of NR2A in complex with glutamate enabled the inclusion of two water molecules in the homology model that are involved in the binding of the charged groups of glutamate into the homology model. The compounds were submitted to a conformational search in Macromodel 9.0 in the tri-ionized state, and the resulting minimized structures were then docked flexibly into a homology model of NR2B. This resulted in similar binding modes for all the compounds, with the amino acid moiety overlapping with that of Glu as seen in our previous study[18] and the deprotonated *N*-hydroxy group receiving an H-bond from the water molecule involved in binding the distal acidic group of Glu. The substituents point like a wedge toward residues H486 and V686, which form a crevice between the upper and lower domains of the clamshell-like ABD structure (Figure 7A). While the ethyl substituent is accommodated by the crevice, the *n*-propyl is in close proximity with residues Lys485 (Figure 7B) and Tyr731 (not shown). In the X-ray crystal structure of NR2A, several water molecules are present in this region and two of them are shown in Figure 7. Furthermore, the *n*-propyl substituent reaches a less conserved region of the ABD. Thus, in the X-ray structure of the ABD of NR2A, Lys485 is in close proximity to the backbone carbonyl of Arg711, which is followed by Gly712. This two-peptide sequence corresponds to Arg712-Gly713 in NR2B, but Arg722-Ser723 in NR2C and Pro736-Arg737 in NR2D. This sequence difference could explain the observed difference in pharmacology of Pr-NHP5G (**6d**) and designing ligands with substituents protruding into this region may lead to NMDA receptor ligands with increased subtype-selectivity as suggested previously.[26]

Discussion

We have synthesized and pharmacologically characterized a series of 4-substituted NHP5G derivatives to identify ligands suitable for investigating the mechanisms governing partial

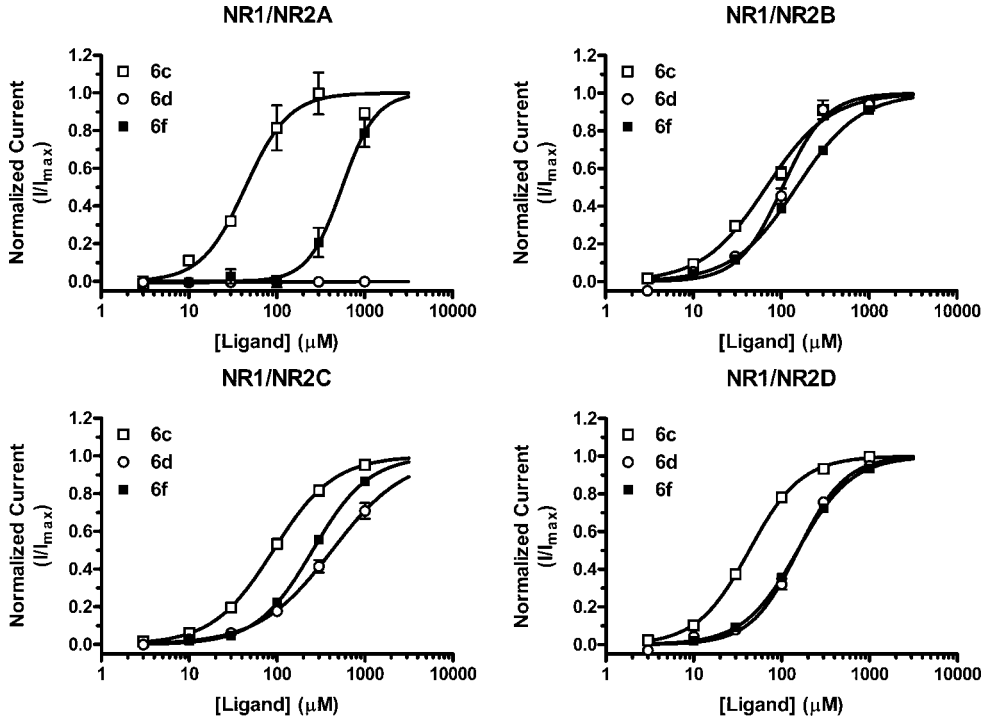

Figure 4. Mean concentration−response curves for racemic compounds Et-(**6c**), Pr- (**6d**), and Cl-NHP5G (**6f**) determined using two-electrode voltage-clamp recordings on *Xenopus* oocytes expressing NR1 in combination with NR2A-D. The curves are normalized to the maximal current response (I_{max}) in the same recording. Data points are represented as mean ± SEM. All EC_{50} values are listed in Table 2.

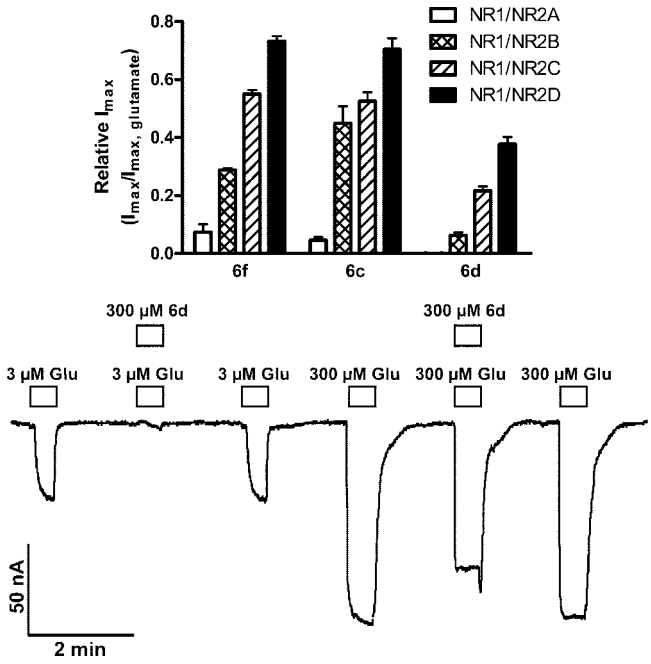

Figure 5. (A) Comparison of maximal currents induced by Et-(**6c**), Pr-(**6d**), and Cl-NHP5G (**6f**) relative to Glu at NR1/NR2A-D subtypes. All bars are represented as mean ± SEM. All relative I_{max} values are listed in Table 2. (B) Representative current responses obtained from a two-electrode voltage-clamp recording on a *Xenopus* oocyte expressing NR1/NR2A receptors. Currents were evoked by Glu alone or coapplication of Glu and Pr-NHP5G at the concentrations indicated above each response.

agonism at the NMDA receptor. This series of NHP5G compounds displays several remarkable properties. All of the compounds are partial agonists at the NMDA receptors with varying degrees of receptor activation. Furthermore, the compounds show marked variation at the various NMDA receptor

Table 3. Potency and Efficacy Relative to Glu of the (*R*)-Form of **6a**−**d** and **6f** at Recombinant NR1/NR2B Receptors Expressed in *Xenopus* Oocytes.[a,24]

compd	R	EC_{50} (μM)	rel I_{max}	n_{Hill}
(*R*)-**6a**	H	14 [14, 15]	0.61 ± 0.02	1.4
(*R*)-**6b**	Me	36 [35, 38]	0.23 ± 0.01	1.6
(*R*)-**6c**	Et	34 [32, 35]	0.46 ± 0.02	1.6
(*R*)-**6d**	n-Pr	63 [59, 68]	0.09 ± 0.004	1.4
(*R*)-**6f**	Cl	58 [55, 62]	0.33 ± 0.01	1.2

[a] Data are from 4−6 oocytes and the numbers in brackets [min, max] indicate mean ± SEM according to a logarithmic distribution.

subtypes both in terms of potency and efficacy. Thus, these compounds highlight the importance of introducing substituents in NMDA receptor ligands that can reach less conserved regions of the receptor. We were able to separate the enantiomers of the racemic mixtures and have been able to determine to a high degree of confidence the absolute configuration from several lines of evidence, including the HPLC elution order, the good agreement between calculated and measured ECD spectra, and the similarity between calculated and experimental NMR spectra of Mosher amide diastereomers of the ethyl compounds. The separation of enantiomers is important because apparent partial agonism can arise from mixed agonistic and antagonistic behavior of opposing enantiomers.[27] However, our data showed that the activity could be attributed to the (*R*)-enantiomers in this series. The unsubstituted (*R*)-**6a** and chloro substituted (*R*)-**6f** have already been employed in a mutagenic study, where it was concluded that steric clashes between the substituents and residues His486 and Val686 were important determinants for the agonist efficacy of the compounds relative to Glu. These two residues form a crevice in the ligand binding domain separating upper and lower domains in the clamshell-like ABD structure, and introducing steric bulk in this region was expected to prevent closure of the ligand binding domain and concomitant receptor activation.

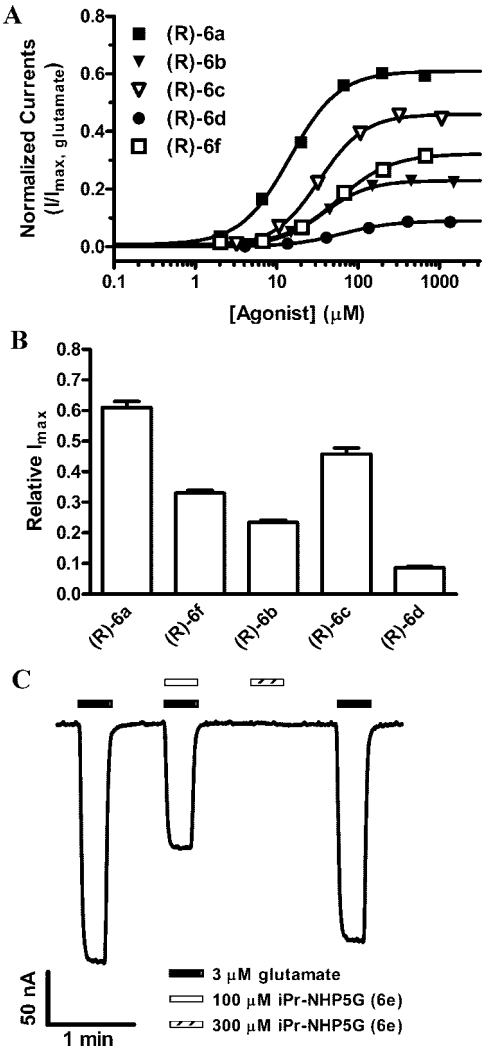

Figure 6. (A) Mean concentration−response curves for compounds (*R*)-**6a**−**d**,**f** (*R* = H, Me, Et, *n*-Pr, Cl, respectively) determined using two-electrode voltage-clamp recordings on *Xenopus* oocytes expressing NR1/NR2B receptors. The curves are normalized to the maximal current response (I_{max}) to Glu in the same recording. Data points are represented as mean ± SEM. All EC_{50} values are listed in Table 3. (B) Bar graph showing the maximal currents (I_{max}) of the ligands relative to the maximal current induced bu Glu. (C) Representative current responses obtained from a two-electrode voltage-clamp recording on a *Xenopus* oocyte expressing NR1/NR2B receptors. Currents were evoked by Glu alone or coapplication of Glu and (*R*)-**6e** at the concentrations indicated above each response.

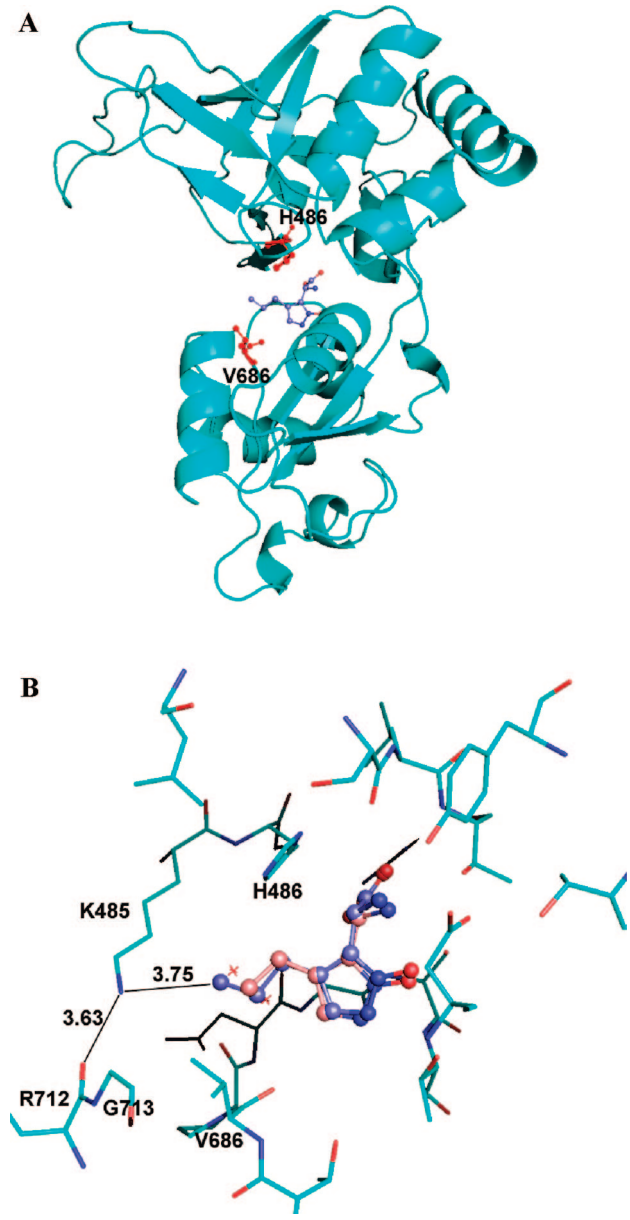

Figure 7. (A) Structure of a homology model of the ABD of NR2B (cyan) containing *n*-Pr-NHP5G ((*R*)-**6d**, blue) showing the residues (red) lining a crevice to the agonist binding site. Previous studies have shown these residues to be important determinants of agonist efficacies of several compounds.[18] (B) Et-NHP5G ((*R*)-**6c**, pink) and *n*-Pr-NHP5G ((*R*)-**6d**, blue) docked in the homology model. The distances from the amino group of Lys485 to the *n*-propyl group and the peptide carbonyl between Arg712 and Gly713 are indicated in Ångstroms. Water molecules are shown as red asterisks.

Completion of the entire series now reveals that the compounds display a trend with respect to substituents that was unexpected on the basis of the mutagenesis study because the efficacy does not completely follow inversely the steric bulk added to the ligands. In particular, the ethyl substituted compound is more efficacious than the methyl substituted compound but still less efficacious compared to the unsubstituted compound, which is surprising considering the increased steric bulk imposed by the ethyl group. Docking the compounds into a homology model of the ABD of NR2B based on the X-ray crystallographic structure of the highly homologous NR2A ABD construct shows that the ethyl group reaches a region where several water molecules are present. Compared with the methyl and chloro groups, displacement of some of these water molecules by the ethyl group could thermodynamically favor a conformation of the ABD that permits receptor activation, offering a plausible explanation for the unusual trend. By contrast, *n*-propyl and isopropyl substituents are in close contact with residues in the receptor, which again is in agreement with steric inhibition of the domain closure.

In conclusion, we have identified a series of analogous selective NMDA receptor ligands that induce various degrees of receptor activation. These compounds may constitute valuable pharmacological tools for studying the mechanisms governing partial agonism at the NMDA receptor. This series shows that factors other than steric hindrance may determine the degree of activation of NMDA receptors. In particular, the *n*-propyl-substituted compound in this series is interesting because it significantly differentiates between NMDA receptors containing different NR2 subunits and therefore offers a promising pharmacological tool for investigating differences in the func-

tional properties of NMDA receptor subtypes at a molecular and cellular level. This could have relevance in several CNS disorders, including schizophrenia. Finally, modeling studies suggest a strategy for designing novel ligands that may be able to discriminate between NMDA receptor subtypes.

Experimental Section

Chemistry. General Methods. All reactions involving air-sensitive reagents were performed under N_2 using syringe-septum cap technique and all glassware was flame-dried prior to use. Flash chromatography (FC) was performed using silica Merck 60 (230−400 mesh). ^{1}H (300 MHz), ^{19}F (282 MHz), and ^{13}C (75 MHz) NMR were recorded on a Varian instrument using TMS and citalopram oxalate as internal standard. HRMS was performed on a JEOL Hx110/110 mass spectrometer. All solvents and reagents were analytical grade purchased from Aldrich or Fluka and used without further purification unless otherwise stated. THF was distilled from Na/benzophenone under N_2. DMF was stored over 3Å molecular sieves. *n*-Buli[28] and *i*-PrMgCl[29] solutions were titrated prior to use. Preparative chiral HPLC was performed using a Crownpak CR(+) column (10 mm × 150 mm, Daicel) equipped with a CR(+) guard column (4.0 mm × 10 mm, Daicel) connected to a HPLC system consisting of a Jasco 880PU pump, a Rheodyne 7125 injector, a TSP UV100 detector set at 234 nm, and a Merck-Hitachi D-2000 chromato-integrator. The column was eluted at r.t. with 1.5 mL/min of aqueous TFA, pH 2. Upon resolvation, the solutions containing the amino acid was collected and lyophilized. Chiral HPLC analyses of the resolved stereoisomers were performed using a Crownpak CR(−) column (4.0 mm × 150 mm, Daicel) equipped with a water-jacket, and generally the enantiomeric purities of the isolated amino acids were >95% unless otherwise indicated. The column was eluted with aqueous $HClO_4$ (pH 1.5 or pH 2.0) at 0.4 mL/min, and the temperature was controlled by a Hetofrig thermostat at 20, 10, or 1 °C. A TSP HPLC system consisting of a P2000 pump, an AS3000 autoinjector, and an SM5000 PDA detector was used for the chiral HPLC analyses.

General Procedure for Metal−Halogen Exchange and Reaction with Aldehyde. 8 (1 mmol) in THF (20 mL) was added to a flame-dried flask, and the resulting solution was cooled to 0 °C. Isopropyl magnesium chloride (1.2 mmol, 2 M in THF) was added dropwise over a period of 5 min, and the resulting mixture was stirred at 0 °C for 1 h. The aldehyde or ketone (1.2 mmol) dissolved in THF (2 mL) was added, and the resulting solution was stirred for an additional 30 min at 0 °C before allowing to warm to r.t. over 30 min and quenched with NH_4Cl (saturated aq, 10 mL). The aqueous phase was extracted with EtOAc (3 × 20 mL), and the combined organic phases were dried over $MgSO_4$ and evaporated in vacuo. FC (PE:EtOAc) afforded the title compound.

1-(1-Benzyloxy-pyrazol-4-yl)-ethanol (9b). From **8** (3.0 g, 10 mmol) and acetaldehyde (0.8 mL, 12 mmol). FC (PE:EtOAc 2:1) afforded 1.47 g (72%) of the title compound.

1-(1-Benzyloxy-pyrazol-4-yl)-propanol (9c). From **8** (3.0 g, 10 mmol) and propanal (1.1 mL, 12 mmol). FC (PE:EtOAc 2:1−1:1) afforded 2.13 g (92%) of the title compound.

2-(1-Benzyloxy-pyrazol-4-yl)-propan-2-ol (9d). From **8** (3.0 g, 10 mmol) and acetone (0.87 mL, 12 mmol). FC (PE:EtOAc 2:1−1:1) afforded 2.14 g (92%) of the title compound.

General Procedure for Dehydroxylation. To a solution of the alcohol (**9a**−**9d**) (1 mmol) and triethylsilane (2 mmol) in $CHCl_3$ (10 mL), trifluoroacetic acid (5 mL) was added dropwise at room temperature, and the resulting solution was stirred at reflux for 2 h. The mixture was cooled, water (10 mL) was added, and the aqueous phase was extracted with diethyl ether (3 × 10 mL). The combined organic phases were dried over $MgSO_4$ and evaporated in vacuo. FC (PE:EtOAc) afforded the title compound.

1-Benzyloxy-4-methylpyrazole (10a). From **9a** (2 g, 9.8 mmol). FC (PE:EtOAc 8:1) afforded 1.45 g (79%) of the title compound.

1-Benzyloxy-4-ethylpyrazole (10b). From **9b** (1.3 g, 6 mmol). FC (PE:EtOAc 8:1) afforded 1.13 g (95%) of the title compound.

1-Benzyloxy-4-propylpyrazole (10c). From **9c** (2.14 g, 9.2 mmol). FC (PE:EtOAc 6:1) afforded 1.71 g (87%) of the title compound.

1-Benzyloxy-4-isopropylpyrazole (10d). From **9d** (2.32 g, 10.8 mmol). FC (PE:EtOAc 6:1) afforded 1.64 g (82%) of the title compound.

1-Benzyloxy-4-chloropyrazole (10e). 1-Benzyloxypyrazole[30] (3 g, 17 mmol) was dissolved in diethyl ether (50 mL) and cooled to −15 °C. Sulfuryl chloride (5 mL, 62 mmol) was added dropwise over 30 min, and the resulting solution stirred for an additional 30 min at 0 °C. Water (20 mL) was slowly added, and the aqueous phase extracted with diethyl ether (3 × 25 mL). The combined organic phases was washed with $NaHCO_3$ (saturated aq, 3 × 25 mL), brine (1 × 25 mL), dried over $MgSO_4$, and evaporated in vacuo to yield 3.51 g of the title compound, which crystallized upon standing in a refrigerator.

General Procedure for the Synthesis of the Protected Amino Acid. To a stirred solution of the benzyloxypyrazole (**10a**−**e**) (1 mmol) in THF (10 mL) at −78 °C, *n*-BuLi (0.75 mL, 1.6 M in hexane, 1.2 mmol) was added dropwise over approximately 2 min. After 5 min, a solution of diethyl *N*-Boc iminomalonate (382 mg, 1.4 mmol) in THF (1 mL) was added and the resulting mixture was stirred at −78 °C for 3 h before quenching with water. The solution was allowed to warm to room temperature, NH_4Cl (satrated aq, 10 mL) was added, the organic phase was separated, and the water phase was extracted with EtOAc (3 × 10 mL). The combined organic layers were dried over $MgSO_4$ and evaporated in vacuo to afford a crude residue, which was purified by FC (PE:EtOAc) to give the title compound containing minor amounts of coeluting diethyl *N*-Boc-iminimalonate. This material was used without further purification.

Diethyl 2-(1-Benzyloxy-4-methyl-pyrazol-5-yl)-2-*tert*-butyloxycarbonylaminomalonate (11a). From **10a** (0.90 g, 4.8 mmol). FC (PE:EtOAc 7:1) afforded 0.91 g (41%) of **11a** as a colorless oil.

Diethyl 2-(1-Benzyloxy-4-ethyl-pyrazol-5-yl)-2-*tert*-butyloxycarbonylaminomalonate (11b). From **10b** (0.92 g, 4.8 mmol). FC (PE:EtOAc 7:1) afforded 1.08 g 50%) of **11b** as a white solid.

Diethyl 2-(1-Benzyloxy-4-propyl-pyrazol-5-yl)-2-*tert*-butyloxycarbonylaminomalonate (11c). From **10c** (1.1 g, 5.1 mmol). FC (PE:EtOAc 4:1) afforded 1.83 g (73%) of **11c** as a white solid.

Diethyl 2-(1-Benzyloxy-4-isopropyl-pyrazol-5-yl)-2-*tert*-butyloxycarbonylaminomalonate (11d). From **10d** (0.96 g, 4.4 mmol). FC (PE:EtOAc 4:1) afforded 1.14 g (53%) of **11d** as a colorless oil.

Diethyl 2-(1-Benzyloxy-4-chloro-pyrazol-5-yl)-2-*tert*-butyloxycarbonylaminomalonate (11e). From **10e** (1 g, 5.7 mmol). FC (PE:EtOAc 6:1−4:1) afforded 2.1 g (76%) of **11e** as a colorless oil.

General Procedure for Debenzylation. The malonate (**11a**−**e**) (1 mmol) was dissolved in MeOH (10 mL). 10% Pd/C (0.05 mmol) was added, and the mixture was vigorously stirred under hydrogen (1 atm) at 0 °C for 30 min, filtered through celite, and evaporated in vacuo to afford the crude product, which was purified by FC (PE:EtOAc) to give the title compound.

Diethyl 2-*tert*-Butyloxycarbonylamino-2-(4-methyl-1-hydroxypyrazol-5-yl)-malonate (12a). From **11a** (624 mg, 1.35 mmol). FC (PE:EtOAc 2:1) afforded 426 mg (85%) of **12a** as a yellowish oil.

Diethyl 2-*tert*-Butyloxycarbonylamino-2-(4-ethyl-1-hydroxypyrazol-5-yl)-malonate (12b). From **11b** (1.0 g, 2.1 mmol). FC (PE:EtOAc 2:1) afforded 789 mg (97%) of 12b as a yellowish oil.

Diethyl 2-*tert*-Butyloxycarbonylamino-2-[4-propyl-1-hydroxypyrazol-5-yl]-malonate (12c). From **11c** (1.71 g, 3.5 mmol). FC (PE:EtOAc 2:1) afforded 1.06 g (97%) of **12c** as a yellowish oil.

Diethyl 2-*tert*-Butyloxycarbonylamino-2-[4-isopropyl-1-hydroxypyrazol-5-yl]-malonate (12d). From **11d** (1.0 g 2.04 mmol). FC (PE:EtOAc 2:1) afforded 1.06 g (97%) of **12d** as a white semisolid.

Diethyl 2-*tert*-Butyloxycarbonylamino-2-(4-chloro-1-hydroxypyrazol-5-yl)-malonate (12e). From **11e** (1.5 g, 3.11 mmol). FC (PE:EtOAc 2:1) afforded 1.08 g (88%) of **12e** as a colorless oil.

General Procedure for Preparation of the Free Amino Acid. To a stirred solution of the malonate (**12a**−**e**) (1 mmol) in THF (10 mL), LiOH (2 M, aq, 9 mmol) was added, and the solution was stirred for 6 h at r.t. The solution was cooled to 0 °C and neutralized with citric acid (10%, aq.). The mixture was extracted with EtOAc (3 × 20 mL), and the combined organic phases were washed with brine (20 mL), dried over $MgSO_4$, and evaporated in vacuo. The resulting residue was stirred in HCl (2 M, 10 mL) at 50 °C for 30 min, and the resulting solution was evaporated to dryness. The product was triturated with Et_2O or CH_3CN to afford a solid that was more >95% pure according to NMR and HPLC. Attempts to recrystallize the compounds resulted in degradation of the products, leading to a less pure material. All the amino acids were separated on a Crownpack CR(+) column with the (*R*)-form eluting first.

Amino-(1-hydroxy-4-methyl-pyrazol-3-yl)-acetic Acid Hydrochloride (6b). From **12a** (281 mg, 0.76 mmol) afforded 153 mg (97%) of **6b** as a white solid.

Amino-(1-hydroxy-4-ethyl-pyrazol-3-yl)-acetic Acid Hydrochloride (6c). From **12b** (759 mg, 1.97 mmol) afforded 247 mg (60%) of **6c** as a pale-yellow solid.

Amino-(1-hydroxy-4-propyl-pyrazol-3-yl)-acetic Acid Hydrochloride (6d). From **12c** (1.06 mg, 2.65 mmol) afforded 450 mg (72%) of **6d** as a white solid.

Amino-(1-hydroxy-4-isopropyl-pyrazol-3-yl)-acetic Acid Hydrochloride (6e). From **12d** (685 mg, 1.71 mmol) afforded 285 mg (71%) of **6e** as a white solid.

Amino-(1-hydroxy-4-chloro-pyrazol-3-yl)-acetic Acid Hydrochloride (6f). From **12e** (1.07 g, 2.7 mmol) afforded 0.536 mg (86%) of **6f** as a white solid.

Molecular Modeling and Ligand−Protein Docking. A homology model of the agonized state of NR2B was constructed based on the soluble NR2A-ABD construct in complex with glutamate (PDB code 2A5S)[11] following the procedure for the NR2B homology model based on NR1 (1PB7). The crystal structure of the soluble NR2A−S1S2 (PDB code 2A5S)[11] was used as a template for the ligand binding domain of NR2B. The sequence of NR2B was aligned with NR2A, truncated, and the GT linker added to form a virtual NR2B−ABD construct containing residues 404−540 followed by the GT linker and residues 662−802. Residues are numbered according to the sequence of total wild type NR2B, including the signal peptide. Using the NR2B construct, a homology model was created using Prime (Schrödinger, Portland, OR) with standard parameters. Van der Waals and electrostatic grids within a $(14Å + 14Å)^3$ box around the ligand position were calculated on this model with the docking code Glide 2.5 (Schrödinger, Portland, OR); default parameters were used, apart from the scaling of nonpolar atoms of the receptor, which was set to 0.9. These grids were then used for ligand docking.

The ligands (*R*)-Et-NHP5G and (*R*)-Pr-NHP5G were submitted to Monte Carlo analysis in tri-ionized forms using the MMFFs force field[31,32] including GB-SA treatment of aqueous solvation in Macromodel 8.1 (Schrödinger, Portland, OR). The global minima of conformations without intramolecular hydrogen bonds of the compounds were flexibly docked with Glide 3.5 to the agonist binding site of the NR2B−S1S2 model. Default parameters were used, apart from the scaling factors of the radii of the nonpolar receptor and ligand atoms, both set to 0.9.

Computational Prediction of Spectra. Initial geometries for the low pH monocationic states of (*S*)-**6b** and (*S*)-**6f** were calculated using OPLS2005 with GB-SA aqueous solvation, and for the Mosher amide of (*S*)-**6c** with chloroform solvation, in Macromodel 9.0 (Schrödinger 2006). For TD-DFT calculations, the conformers were first optimized at B3LYP/6-311+G(d,p), and excitations calculated at the same level of theory, with IEF-PCM treatment of aqueous solvation, in Gaussian'03 (Gaussian 2003). Gaussian line broadening with a half-width of 0.2 eV was used to transform rotatory velocities to simulated spectra. NMR calculations were conducted on the optimized geometries at B3LYP/6-311+G(d,p) with solvation by chloroform (PB-SCRF model) in Jaguar 7.0 (Schrödinger 2006), with magnetic shielding tensors calculated in gas phase at the same level of theory. Correlation coefficients were calculated between experimental and calculated shifts of all protons relative to TMS at the same level of theory, neglecting the five phenyl protons, which are of little value in distinguishing the diastereomers.

In Vitro Pharmacology. Receptor Binding Assays. Affinities for native AMPA, KA, and NMDA receptors in rat cortical synaptosomes were determined using 5 nM [^{3}H]AMPA (45.5 Ci/mmol),[33] 5 nM [^{3}H]KA (47.0 Ci/mmol),[34] and 2 nM [^{3}H]CGP 39653 (K_d = 6 nM, 50.0 Ci/mmol),[35] respectively, with minor modifications as previously described.[36] Rat brain membrane preparations used in these receptor binding experiments were prepared according to a method previously described.[37]

Two-Electrode Voltage-Clamp Electrophysiology. For expression in *Xenopus* oocytes, rat NR1 (GenBank U11418) cDNA was subcloned into pCI-IRES-neo[38] or pGEMHE vectors. The open reading frames of rat NR2A (GenBank D13211), NR2B (M91562), NR2C (D13212), and NR2D (D13214) cDNAs were subcloned into pCI-IRES-bla[38] or pCI-neo (NR2A), pBluescript (NR2B), SP6 (NR2C-D) vectors. *Xenopus* oocytes and cRNA for injection were prepared as previously described.[39] Two-electrode voltage-clamp recordings were performed essentially as previously described.[39] During recordings, the oocytes were voltage-clamped at −60 to −40 mV and continuously perfused at 23 °C with extracellular solution containing (in mM) 90 NaCl, 0.5 $BaCl_2$, 1 KCl, 0.01 EDTA, and 10 HEPES (pH 7.6); 20 μM glycine was included in the extracellular solution at all times.

Agonist concentration−response data for individual oocytes were fitted to the Hill equation. The log EC_{50} and n_H from the individual oocytes were used to calculate the mean ± SEM. For graphical presentation, data sets from individual oocytes were normalized to the maximal response evoked by glutamate in the same recording. The mean ± SEM was calculated for each of the normalized data points. The averaged data points were then fitted to the Hill equation and plotted together with the resulting curve. Relative I_{max} was calculated from a full concentration−response measurement as $I_{max,agonist}/I_{max,glutamate}$, where $I_{max,agonist}$ is the fitted value according to the Hill equation and $I_{max,glutamate}$ is the maximal response evoked by glutamate in the same recording.

Acknowledgment. Lars Skov and Michael Gajhede are acknowledged for their help with CD measurements. We thank Kimberly Haustein and Phuong Le for excellent technical assistance. We thank Drs. S. Heinemann (Salk Institute), S. Nakanishi (Kyoto University), and P. Seeburg (University of Heidelberg) for sharing cDNA encoding the NMDA receptor subunits. Tommy Liljefors is acknowledged for fruitful discussions on modeling and design. This work was supported by NIH (S.F.T.), the Carlsberg Foundation (C.C.), the Alfred Benzon Foundation (K.B.H.), Villum Kann Rasmussen Foundation (K.B.H.), the Lundbeck Foundation (K.B.H.), the Drug Research Academy (N.M.), and the Augustinus Foundation (H.B.O.).

Supporting Information Available: Routine NMR spectra, routine NMR data, preparation of Mosher amides, CD spectra, HPLC traces, and table of purity data. This material is available free of charge via the Internet at http://pubs.acs.org.

References

(1) Bräuner-Osborne, H.; Egebjerg, J.; Nielsen, E.Ø.; Madsen, U.; Krogsgaard-Larsen, P. Ligands for glutamate receptors: Design and therapeutic prospects. *J. Med. Chem.* **2000**, *43*, 2609–2645.
(2) Dingledine, R.; Borges, K.; Bowie, D.; Traynelis, S. F. The Glutamate Receptor Ion Channels. *Pharmacol. Rev.* **1999**, *51*, 7–62.
(3) Erreger, K.; Chen, P. E.; Wyllie, D. J.; Traynelis, S. F. Glutamate receptor gating. *Crit. Rev. Neurobiol.* **2004**, *16*, 187–224.
(4) Riedel, G.; Platt, B.; Micheau, J. Glutamate receptor function in learning and memory. *Behav. Brain Res.* **2003**, *140*, 1–47.
(5) Javitt, D. C. Glutamate as a therapeutic target in psychiatric disorders. *Mol. Psychiatry* **2004**, *9*, 984–997.
(6) Parsons, C. G.; Danysz, W.; Quack, G. Glutamate in CNS disorders as a target for drug development: an update. *Drug News Perspect.* **1998**, *11*, 523–569.

(7) Armstrong, N.; Gouaux, E. Mechanisms for activation and antagonism of an AMPA-sensitive glutamate receptor: crystal structures of the GluR2 ligand binding core. *Neuron* **2000**, *28*, 165–181.
(8) Armstrong, N.; Sun, Y.; Chen, G. Q.; Gouaux, E. Structure of a glutamate-receptor ligand-binding core in complex with kainate. *Nature* **1998**, *395*, 913–917.
(9) Mayer, M. L. Crystal structures of the GluR5 and GluR6 ligand binding cores: molecular mechanisms underlying kainate receptor selectivity. *Neuron* **2005**, *45*, 539–552.
(10) Naur, P.; Vestergaard, B.; Skov, L. K.; Egebjerg, J.; Gajhede, M.; Kastrup, J. S. Crystal structure of the kainate receptor GluR5 ligand-binding core in complex with (*S*)-glutamate. *FEBS Lett.* **2005**, *579*, 1154–1160.
(11) Furukawa, H.; Gouaux, E. Mechanisms of activation, inhibition and specificity: crystal structures of the NMDA receptor NR1 ligand-binding core. *EMBO J.* **2003**, *22*, 2873–2885.
(12) Jin, R.; Banke, T. G.; Mayer, M. L.; Traynelis, S. F.; Gouaux, E. Structural basis for partial agonist action at ionotropic glutamate receptors. *Nat. Neurosci.* **2003**, *6*, 803–810.
(13) Frandsen, A.; Pickering, D. S.; Vestergaard, B.; Kasper, C.; Nielsen, B. B.; Greenwood, J. R.; Campiani, G.; Fattorusso, C.; Gajhede, M.; Schousboe, A.; Kastrup, J. S. Tyr702 is an important determinant of agonist binding and domain closure of the ligand-binding core of GluR2. *Mol. Pharmacol.* **2005**, *67*, 703–713.
(14) Inanobe, A.; Furukawa, H.; Gouaux, E. Mechanism of partial agonist action at the NR1 subunit of NMDA receptors. *Neuron* **2005**, *47*, 71–84.
(15) Cali, P.; Begtrup, M. Synthesis of 1-hydroxypyrazole glycine derivatives. *Tetrahedron* **2002**, *58*, 1595–1605.
(16) Clausen, R. P.; Hansen, K. B.; Cali, P.; Nielsen, B.; Greenwood, J. R.; Begtrup, M.; Egebjerg, J.; Bräuner-Osborne, H. The respective *N*-hydroxypyrazole analogues of the classical glutamate receptor ligands ibotenic acid and (*R*,*S*)-2-amino-2-(3-hydroxy-5-methyl-4-isoxazolyl)acetic acid. *Eur. J. Pharmacol.* **2004**, *499*, 35–44.
(17) Jørgensen, C. G.; Bräuner-Osborne, H.; Nielsen, B.; Kehler, J.; Clausen, R. P.; Krogsgaard-Larsen, P.; Madsen, U. Novel 5-substituted 1-pyrazolol analogues of ibotenic acid: synthesis and pharmacology at glutamate receptors. *Bioorg. Med. Chem.* **2007**, *15*, 3524–3538.
(18) Hansen, K. B.; Clausen, R. P.; Bjerrum, E. J.; Bechmann, C.; Greenwood, J. R.; Christensen, C.; Kristensen, J. L.; Egebjerg, J.; Brauner-Osborne, H. Tweaking Agonist Efficacy at *N*-Methyl-D-aspartate Receptors by Site-Directed Mutagenesis. *Mol. Pharmacol.* **2005**, *68*, 1510–1523.
(19) Felding, J.; Kristensen, J.; Bjerregaard, T.; Sander, L.; Vedsø, P.; Begtrup, M. Synthesis of 4-Substituted 1-(Benzyloxy)pyrazoles via Iodine-Magnesium Exchange of 1-(Benzyloxy)-4-iodopyrazole. *J. Org. Chem.* **1999**, *64*, 4196–4198.
(20) Akoka, S.; Barantin, L.; Trierweiler, M. Concentration measurement by proton NMR using the ERETIC method. *Anal. Chem.* **1999**, *71*, 2554–2557.
(21) Shinbo, T.; Yamaguchi, T.; Nishimura, K.; Sugiura, M. Chromatographic-Separation of Racemic Amino-Acids by Use of Chiral Crown Ether-Coated Reversed-Phase Packings. *J. Chromatogr.* **1987**, *405*, 145–153.
(22) de Leon, C. A. P.; Sutton, K. L.; Caruso, J. A.; Uden, P. C. Chiral speciation of selenoamino acids and selenium enriched samples using HPLC coupled to ICP-MS. *J. Anal. At. Spectrom.* **2000**, *15*, 1103–1107.
(23) Hawkins, C. L.; Lawrance, G. A. Circular dichroism spectra of *N*,*N*-Dimethyl-L-amino acids. *Aust. J. Chem.* **1973**, *26*, 1801–1803.
(24) Christopoulos, A. Assessing the distribution of parameters in models of ligand-receptor interaction: to log or not to log. *Trends Pharmacol. Sci.* **1998**, *19*, 351–357.
(25) Furukawa, H.; Singh, S. K.; Mancusso, R.; Gouaux, E. Subunit arrangement and function in NMDA receptors. *Nature* **2005**, *438*, 185–192.
(26) Kinarsky, L.; Feng, B. H.; Skifter, D. A.; Morley, R. M.; Sherman, S.; Jane, D. E.; Monaghan, D. T. Identification of subunit- and antagonist-specific amino acid residues in the *N*-methyl-D-aspartate receptor glutamate-binding pocket. *J. Pharmacol. Exp. Ther.* **2005**, *313*, 1066–1074.
(27) Ebert, B.; Lenz, S.; Brehm, L.; Bregnedal, P.; Hansen, J. J.; Frederiksen, K.; Bøgesø, K. P.; Krogsgaard-Larsen, P. Resolution, absolute stereochemistry, and pharmacology of the *S*-(+)- and *R*-(−)-isomers of the apparent partial AMPA receptor agonist (*R*,*S*)-2-amino-3-(3-hydroxy-5-phenylisoxazol-4-yl)propionic acid [(*R*,*S*)-APPA]. *J. Med. Chem.* **1994**, *37*, 878–884.
(28) Suffert, J. Simple Direct Titration of Organo-Lithium Reagents Using *N*-Pivaloyl-Ortho-Toluidine and Or *N*-Pivaloyl-*ortho*-Benzylaniline. *J. Org. Chem.* **1989**, *54*, 509–510.
(29) Lin, H. S.; Paquette, L. A. A Convenient Method for Determining the Concentration of Grignard-Reagents. *Synth. Commun.* **1994**, *24*, 2503–2506.
(30) Vedsø, P.; Begtrup, M. Synthesis of 5-Substituted 1-Hydroxypyrazoles Through Directed Lithiation of 1-(Benzyloxy)Pyrazole. *J. Org. Chem.* **1995**, *60*, 4995–4998.
(31) Halgren, T. A. MMFF VI. MMFF94s option for energy minimization studies. *J. Comput. Chem.* **1999**, *20*, 720–729.
(32) Halgren, T. A. MMFF VII. Characterization of MMFF94, MMFF94s, and other widely available force fields for conformational energies and for intermolecular-interaction energies and geometries. *J. Comput. Chem.* **1999**, *20*, 730–748.
(33) Honore, T.; Nielsen, M. Complex structure of quisqualate-sensitive glutamate receptors in rat cortex. *Neurosci. Lett.* **1985**, *54*, 27–32.
(34) Braitman, D. J.; Coyle, J. T. Inhibition of [^{3}H]kainic acid receptor binding by divalent cations correlates with ion affinity for the calcium channel. *Neuropharmacology* **1987**, *26*, 1247–1251.
(35) Sills, M. A.; Fagg, D.; Pozza, M.; Angst, C.; Brundish, D. E.; Hurt, S. D.; Wilusz, E. J.; Williams, M. [^{3}H]CGP 39653: a new *N*-methyl-D-aspartate antagonist radioligand with low nanomolar affnity in rat brain. *Eur. J. Pharmacol.* **1991**, *192*, 19–24.
(36) Hermit, M. B.; Greenwood, J. R.; Nielsen, B.; Bunch, L.; Jørgensen, C. G.; Vestergaard, H. T.; Stensbøl, T. B.; Sanchez, C.; Krogsgaard-Larsen, P.; Madsen, U.; Bräuner-Osborne, H. Ibotenic acid and thioibotenic acid: a remarkable difference in activity at group III metabotropic glutamate receptors. *Eur. J. Pharmacol.* **2004**, *486*, 241–250.
(37) Ransom, R. W.; Stec, N. L. Cooperative modulation of [^{3}H]MK801 binding to the *N*-methyl-D-aspartate receptor ion channel complex by L-glutamate, glycine and polyamines. *J. Neurochem.* **1988**, *51*, 830–836.
(38) Hansen K. B.; Bräuner-Osborne H.; Egebjerg J. Pharmacological characterization of ligands at recombinant NMDA receptor subtypes by electrophysiological recordings and intracellular calcium measurements *Comb. Chem. High Throughput Screen.* **2008**, *11*, in press.
(39) Traynelis, S. F.; Burgess, M. F.; Zheng, F.; Lyuboslavsky, P.; Powers, J. L. Control of voltage-independent zinc inhibition of NMDA receptors by the NR1 subunit. *J. Neurosci.* **1998**, *18*, 6163–6175.

JM800025E